



High-performance visible light photocatalytic activity of cobalt (Co) doped CdS nanoparticles by wet chemical route

N. Jeevanantham¹ · O. N. Balasundaram¹

Received: 29 May 2018 / Accepted: 10 September 2018
© Iranian Chemical Society 2018

Abstract

The role of cobalt (Co) dopant on structural, morphological, optical and photocatalytic properties of CdS nanoparticles were methodically reported. XRD analysis confirms that both pure and Co-doped CdS samples have cubic structure with no impurity phases detected and the results are good in agreement with the standard JCPDS value (Card No. 80-0019). TEM images reveal the spherical morphology with an average diameter of around 15–35 nm. A noticeable red-shift of absorption edge and bandgap narrowing can be attributed to the inclusion of cobalt ions and creation of defect levels in the bandgap, which is confirmed by UV analysis. Photoluminescence spectra show defects-free nature of synthesized nanoparticles. The functional groups and chemical interaction were determined by FTIR spectra. The photodegradation of MB dye with Co-doped CdS is more efficient under visible light compared to pure CdS. The 15 mol% Co-doped CdS acts as an efficient photocatalyst. The presence of Co²⁺ generated electron and holes and prolonged the recombination rate by introducing the temporary trapping sites, which essentially causes to improve the photocatalytic efficiency of the synthesized samples. The possible photocatalytic mechanism by Co doping is also discussed in detail.

Keywords CdS · Co doping · Methylene blue · Optical property · Visible light · Catalyst

Introduction

Emerging investigation of nanotechnology has resulted in the classification of many unique properties of nanomaterials such as enhanced magnetic, catalytic, optical, electrical and mechanical properties when compared to conventional formulations of the same material. The learning about semiconductor nanoparticles has been an interesting field of research for more than 2 decades. This is because it gives an opportunity to understand the physical properties in low dimensions and to explore their vast potential for applications, e.g. in optoelectronics [1–4]. Semiconductor nanoparticles have been paid much attention during the past 2 decades owing to their unique size-dependent chemical and physical properties. Among the different types of semiconducting nanoparticles (ZnS, SnS, InS, and CdSe), CdS is one of the great semiconducting nanoparticles and potential applications as nanoelectronics and photocatalytic materials

are having a relatively large nonlinear optical response and photocatalytic activity. Since their properties and structures are closely related to size, shape and dimension play important role to determine their physical properties. Many researchers have doped ‘d’ group elements like Mn, Cr and Fe into the host matrices of CdS nanocrystals and investigated the properties possessed by the material [5–8]. Generally, the effective dopant can modify the structural and electronic properties of the pure CdS nanoparticles, which results in enhancing their photocatalytic activity.

Chauhan et al. [9] have prepared Mn-doped CdS nanoparticles using simple chemical precipitation method and studied the photocatalytic properties. Ertis et al. [10] have investigated the effect of Sb dopant on structural, optical and photocatalytic properties. They also reported Sb-doped CdS showed superior photocatalytic properties toward MB dye than pure CdS. Abdulkarem et al. [11] also reported the indium (In)-doped CdS by using one step hydrothermal method. They also proved In-doped CdS enhanced the photocatalytic activity of RhB under visible light irradiation. A large number of reports are available on the CdS-based DMSs with transition metals other than cobalt and less concentration about its photocatalytic properties. For example,

✉ O. N. Balasundaram
balupsg02@gmail.com

¹ Department of Physics, PSG College of Arts and Science, Coimbatore, Tamilnadu 641 014, India

Tambidurai and his co workers reported structural, optical and electrical properties of CdS:Co nanoparticles [12, 13], but they have not studied the magnetic and photocatalytic properties. Saravanan et al. reported RTFM in CdS:Co nanoparticles synthesized by chemical co precipitation method [14]. Strong RTFM in Co-doped CdS nanocrystals synthesized by gas liquid phase mechanism was reported by Tingtinghu [15]. Most of the earlier reports are on the wurtzite structure of CdS:Co DMSs and studied the structural and electronics properties. In an attempt to further improve the photocatalytic activity, we doped Co into CdS. The role of Co dopant has also positive influence on the structural, optical and photocatalytic properties. To the best of the author's knowledge this is the first preliminary report about structural, optical and photocatalytic properties of Co-doped CdS nanoparticles by simple wet chemical route.

Experimental procedure

Materials

Cadmium acetate dehydrate $\text{Cd}(\text{CH}_3\text{COO})_2 \cdot 2\text{H}_2\text{O}$, sodium sulfide ($\text{Na}_2\text{S} \cdot 2\text{H}_2\text{O}$), cobalt sulfate ($\text{CoSO}_4 \cdot 2\text{H}_2\text{O}$) for source materials for CdS and Co respectively. The chemicals were purchased from Merck, India. All the chemicals used were of analytical grade and were used as received without any further purification.

Preparation of Co-doped CdS

Pure CdS and Co-doped CdS nanoparticles have been synthesized through chemical precipitation technique. Aqueous solution of cadmium acetate dehydrate $\text{Cd}(\text{CH}_3\text{COO})_2 \cdot 2\text{H}_2\text{O}$ and required amount of cobalt sulfate were stirred for 1 h at room temperature. The concentration of Co is varied from 5 to 15 mol%. To this mixture, 20 ml of ethanol was further added and allowed for 6 h stirring. The NH_4OH (as precipitate agent) solution was added dropwise until the pH value reaches 11. During this process the drop rate must be controlled in order to maintain the chemical homogeneity. The entire solution turned into deep green in color and further allowed to stir for 48 h which in optimized aging period of the growth process. The dark green final products were washed thoroughly with the organic solvents (acetone, ethanol) and dried at 160 °C in a hot air oven and preserved in moisture-free container. The dark green final products were washed thoroughly with the organic solvents (acetone, ethanol) and dried at 60 °C in a hot air oven and preserved in moisture-free container. The pure CdS nanoparticles were prepared in a similar manner without use of Sm source.

Characterization techniques

Powder X-ray diffraction method with Rigaku X-ray diffractometer with monochromatic $\text{Cu K}\alpha$ radiation of wavelength 1.5406 Å) was used to analyze the crystallographic nature and grain size of the as-synthesized products. TEM was recorded with JEM2100 model. High-resolution electron microscope was recorded with accelerating voltage of 200 kV. The elemental analysis of the samples was performed using EDS spectra (JEOL Model JED-2300). UV-vis absorption spectra were taken on a Perkin-Elmer Lambda 2 spectro-meter. Photoluminescence spectra of the samples were recorded using PerkinElmer LS 55 spectrometer equipped with a He-Cd laser source, Excitation length used was 325 nm. The functional groups were analyzed by using Fourier transformed infrared spectra (FT-IR), which is collected using a 5DX FTIR spectrometer.

Photocatalytic setup

A specially designed photocatalytic reactor system made of double-walled reaction chamber of glass tubes was used for photodegradation experiments. A 300 W xenon lamp as used for the UV light source and the control of the reaction bottle of the plane window is placed at 20 cm from the xenon lamp. The photocatalytic degradation reactions of MB and RHB were considered from the model pollutants. 50 mg of the prepared photocatalyst was mixed with 50 mL of aqueous solution containing the appropriate dye (10 mg/L for MB and RHB). Prior to reactions, the dye solution with catalysts was stirred in the dark for 30 min to attain the adsorption, desorption equilibrium. The concentration of the aqueous suspensions (MB and RHB) in each sample was analyzed using UV-vis spectrophotometer at a wavelength of 664 nm. The photocatalytic efficiency was calculated from the expression $\eta = (1 - C/C_0)$, where C_0 is the concentration of dyes (MB and RHB) before illumination and C is the concentration of dyes after a certain irradiation time. The time interval of irradiation time was 20 min.

Results and discussion

XRD analysis

The structural perfection of the as synthesized pure and Co-doped CdS nanoparticles was analyzed through XRD spectra and the corresponding profile shown in Fig. 1a). The XRD patterns indicate that both pure and Co-doped CdS samples were composed of single cubic structure. The XRD pattern of pristine CdS sample exhibit peaks at

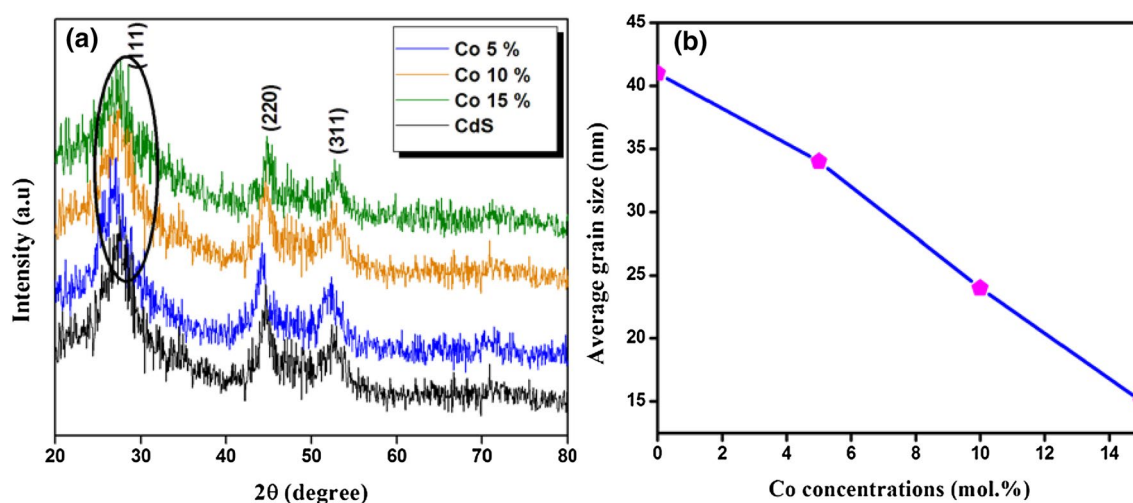


Fig. 1 **a** Powder XRD pattern of pure and Co-doped CdS nanoparticles. **b** Variation grain size as a function of Co content

2θ values 26.2° , 44.1° and 51.4° which could be indexed to scattering from (111), (220) and (311) planes with measured d -spacing 3.32, 2.07 and 1.73 Å of all crystal planes of the cubic structure. All the diffraction peaks are in agreement with the reported JCPDS Card No. 80-0019. No other impurity phases were detected, which indicates that the incorporation of Co^{2+} in the CdS matrix does not introduce considerable change in the crystal structure except expansion and distortion of the crystal lattice. But the clear shift was observed in the peak position. The peak position of pure CdS was shifted towards the longer angle side ($\sim 0.5^\circ$) with the increase of Co content. The lattice constants of Co (15%) doped CdS nanoparticles are found to be $a = 4.1145$ Å and $c = 6.6128$ Å, which are higher than that of 5% doped CdS ($a = 4.1101$ Å and $c = 6.6102$ Å). This is due to that the ionic radius of Co (0.74 Å) is smaller than that of Cd (0.96 Å) [16]. The result suggests that the doped Co atoms substitute for Cd atoms. The grain size has been calculated using Scherrer's formula [17].

$$d = \frac{K\lambda}{\beta \cos \theta}$$

where d is the mean crystallite size, K is the shape factor taken as 0.89, λ is the wavelength of the incident beam, β is the full width at half maximum and θ is the Bragg angle. The average crystalline size was calculated as 41, 34, 24 and 15 nm for pure and Co-doped CdS nanoparticles, respectively. This result suggests that the grain growth is suppressed due to doping of Co into Cd-site. For clear understanding, we plotted the graph between crystalline size as a function of Co concentrations and the corresponding spectrum is shown in Fig. 1b.

TEM with EDS analysis

The shape and size of pure and Co-doped CdS nanostructures were investigated using TEM measurements. Figure 2a–c shows the TEM micrographs of pure and Co-doped CdS nanostructures. The morphology of the samples was in spherical-shaped and the average diameter was found to be decreased with the increase of Co content. The decrease of grain size by Co doping was also confirmed by XRD results. The average particle size was found as 40, 25 and 16 nm for pure and Co (10 and 15 mol%) doped CdS nanoparticles, respectively. Concentric circles of SAED pattern correspond to the (111), (220) and (311) planes of cubic phase, revealing the small size of the synthesized nanoparticles (Fig. 2d). These results were in good agreement with the XRD results. The elemental composition of the Co (15%) doped CdS nanoparticles was analyzed by EDS and the corresponding figure shown in Fig. 2e. An EDX result (Fig. 2e) gives the strong K diffraction peaks at 3.1, 3.3 and 2.3 keV, corresponding to the elemental S and Cd and the diffraction peaks at 0.9 and 6.5 keV corresponding to the cobalt element present in the materials. The Cu element was found in the composition, due to the grid used for EDS measurements.

UV–vis absorption spectra analysis

The optical properties of the nanoparticles were analyzed using UV–vis absorption spectra analysis. Figure 3a shows the UV–vis absorption spectra of pure and Co-doped CdS nanoparticles with different Co content. It can be seen that the optical absorption edge was shifted towards the longer wavelength side. A considerable red-shift of absorption

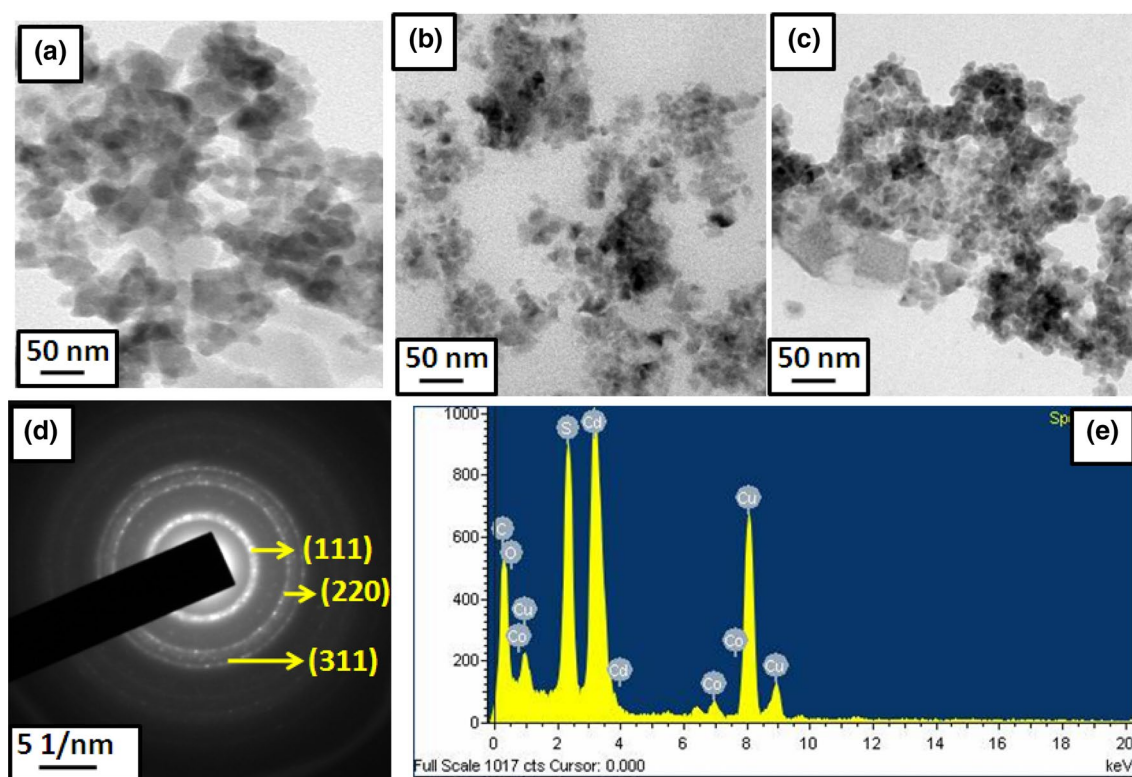


Fig. 2 TEM images of **a** pure CdS, **b** 10% Co, **c** 15% Co, **d** corresponding SAED pattern. **e** EDS spectra of 15% Co-doped CdS nanoparticles

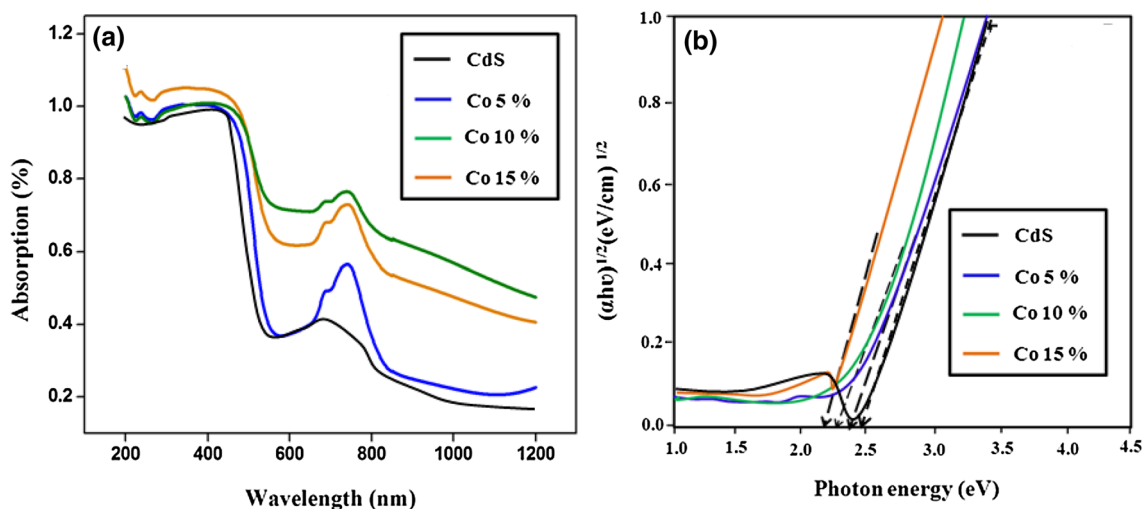


Fig. 3 **a** UV-vis absorptions spectra of pure and Co-doped CdS nanoparticles. **b** Bandgap determination

edge with increasing cobalt concentration indicates the bandgap narrowing. This may be due to increase in the carrier concentration by the inclusion of cobalt ions and creation of defect levels in the bandgap. The optical band gap energy was calculated using Tauc relation [18]. The relation between the absorption coefficient (α) and optical band gap (E) can be written as Eq. (1) [19]:

$$(\alpha hv)^2 = C (hv - E), \quad (1)$$

where the optical band gap for the absorption edge can be attained by extrapolating the linear portion of the plot (Fig. 3b). The optical band gap decreases from 2.49 to 2.19 eV with increasing Co concentration. The decrement of energy band gap is mainly due to $sp-d$ exchange interaction

between the band electrons and the localized d electrons of Co^{2+} ions doped for CdS ions [20]. This similar phenomenon was observed by Parthibavarman et al. [21] using Co-doped SnO_2 nanoparticles synthesized via microwave irradiation method.

Photoluminescence spectra analysis

Photoluminescence (PL) study has been carried out to obtain information regarding electronic transitions associated with dopant, impurities, if any, and defects present in the synthesized nanoparticles. The PL spectrum was observed in the range from 300 to 600 nm excitation wavelengths of the CdS nanoparticles with Co concentrations (0.05–0.15 mol%) is shown in Fig. 4. It was noted that all the samples exhibited the emission peaks at 361 and 451 nm that are usually observed from the excitonic emission luminescence and blue emission band was associated with the emission due to electronic transition from the conduction band to an acceptor level due to Co concentration [22]. The luminescence intensity was found to increase drastically when increasing the Co content. Here Co acts as the sensitizing agent and is responsible for the enhancement of radiative recombination process. Moreover, shift in the emission peak and increase in the peak intensity can be attributed to the variation of position of the defect levels within the band gap. The defect (decrease) in the band gap was also confirmed by UV spectra analysis.

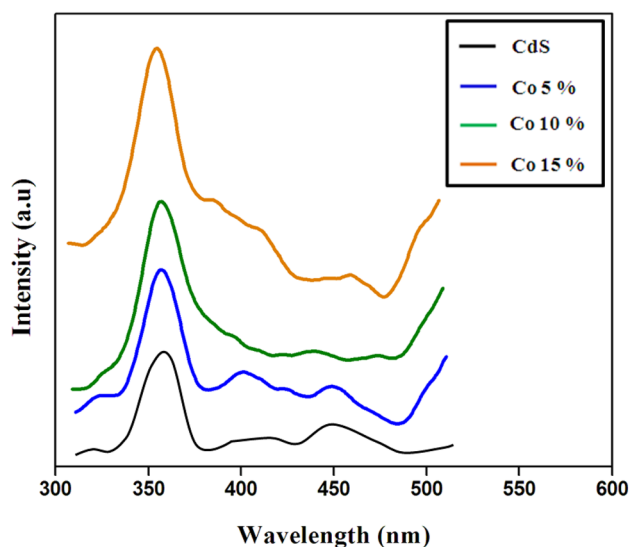


Fig. 4 Room temperature photoluminescence spectra of pure and Co-doped CdS nanoparticles

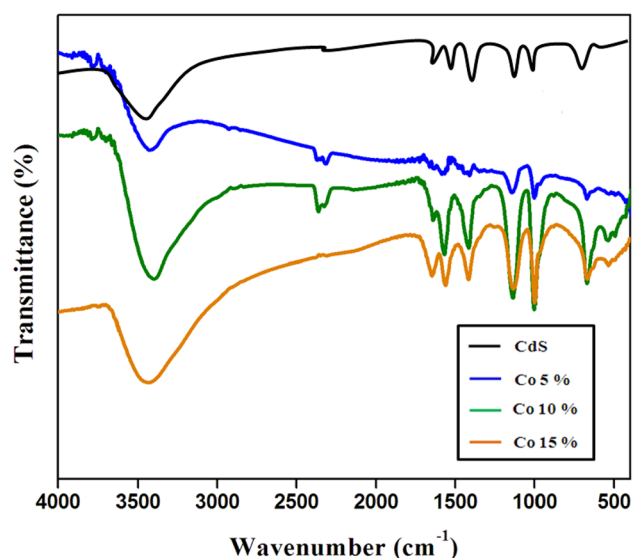


Fig. 5 FTIR spectra of pure and Co-doped CdS nanoparticles

FTIR spectra analysis

The functional groups and bonding information was analyzed through FTIR spectrum. Figure 5 shows the FTIR spectra of pure and Co-doped CdS nanoparticles. It can be seen that there may be some adsorbed water vapor which leads to a broad intermolecular hydrogen bonded O–H stretch around 3453 cm^{-1} . This may be due to the atmospheric moisture. The peaks at 1650 cm^{-1} , 1417 cm^{-1} are assigned to the vibrational mode of OH bending [23, 24]. The peaks located at 994 and 692 cm^{-1} are ascribed to asymmetric stretching of CdS. These modes indicate the presence of resonance interaction between vibration modes of CdS ions in the crystal. The absence of any peaks related to Co again supported that Co has successfully doped with CdS nanoparticles.

Photocatalytic studies

Absorbance and visible light driven photocatalytic test

To get the response of photocatalytic activities of Co-doped CdS, the absorption spectra of exposed samples at various time intervals were recorded and the rate of decolorization was observed in terms of change in intensity at λ_{max} of the dye. The absorption spectra of the aqueous solution of MB and RhB dyes were irradiated under visible light. The intensity of all the samples was completely disappearing in 120 min irradiation of visible light. Hence, we concluded that these samples are more photo active material under visible light conditions.

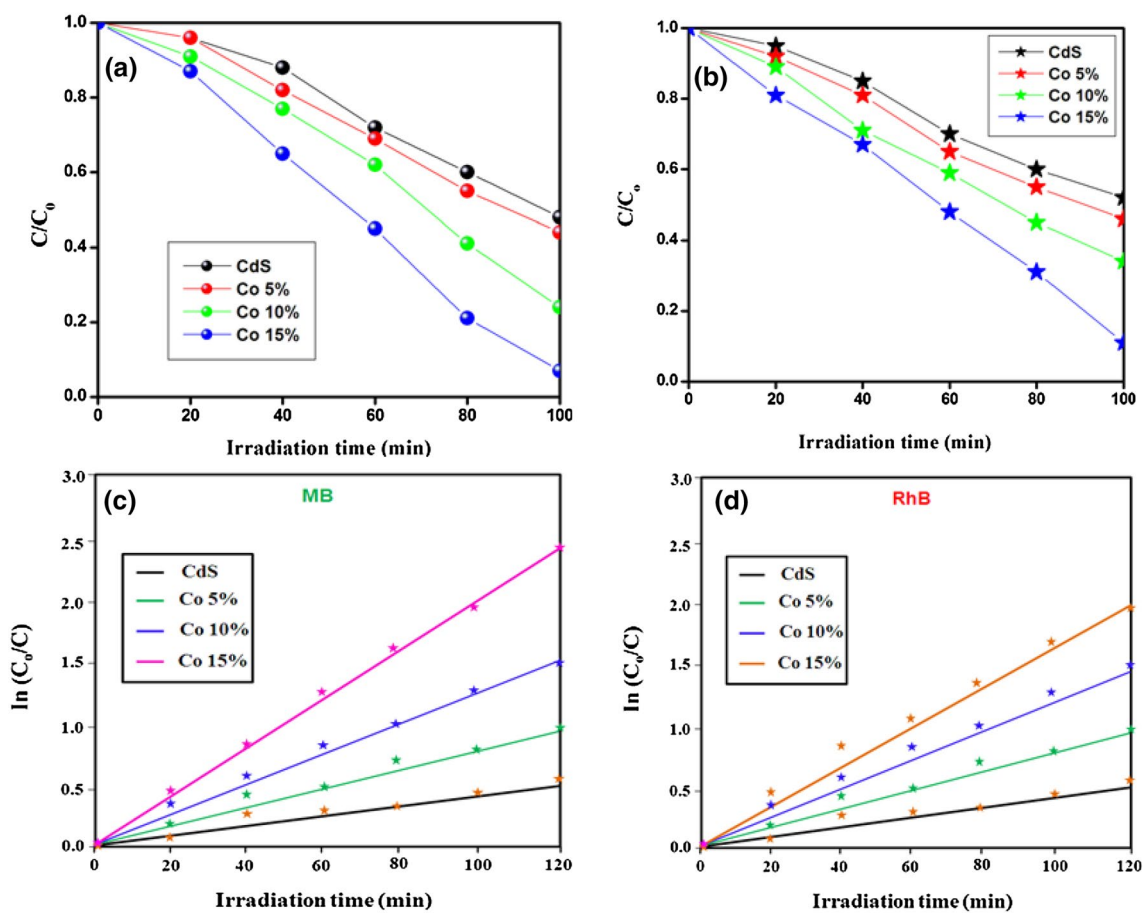


Fig. 6 Temporal degradation profile of **a** MB and **b** RhB and Kinetic degradation test of **c** MB and **d** RhB using pure and Co-doped CdS catalysts under visible light irradiation

Degradation efficiency test

The samples were further tested for degradation efficiency under visible light irradiation with a regular interval of 20 min and the corresponding temporal graph is shown in Fig. 6a, b. It was clearly evident that the degradation of dye solutions linearly decreases with the increase of visible light irradiation. The MB degradation efficiency was found to be 48, 56, 76 and 93% for pure CdS, 5, 10 and 15 mol% Co-doped CdS, respectively. Similarly, the RhB degradation efficiency was found to be 45, 54, 66 and 89% for pure CdS, 5, 10 and 15 mol% Co-doped CdS, respectively. In both cases, Co 15% doped CdS samples showed highest photocatalytic performance than other samples. This may be due to the high surface area and smaller crystalline nature. Moreover, the Co–CdS with the appropriate band gap in the nanosized materials can enable transfer of electrons and holes to the surface under light illumination; these electrons and holes can improve the photoreaction.

Kinetic study

The pseudo first-order kinetic model was used for determination of reaction rate constant (k) of MB and RhB, which is expressed by Eq: $\ln C/C_0 = -kt$ [25]. This model is normally used for the photocatalytic degradation process when the initial concentration of the pollutant is low. Figure 6c, d depicts the $\ln(C/C_0)$ versus the irradiation time for different as prepared photocatalysts. Pure CdS catalyst reaction rate constant k was found to be 0.0015 min^{-1} , under the irradiation of visible light, while Co 15 (mol%) showed the maximum reaction rate constant (0.0088 min^{-1}), which is 4.5 times that of pure CdS.

Recycle test

Figure 7 shows the repeatability test of pure CdS and Co (15 mol%) doped CdS photocatalyst for the degradation of MB and RhB. Figure 7 confirms the reusability and

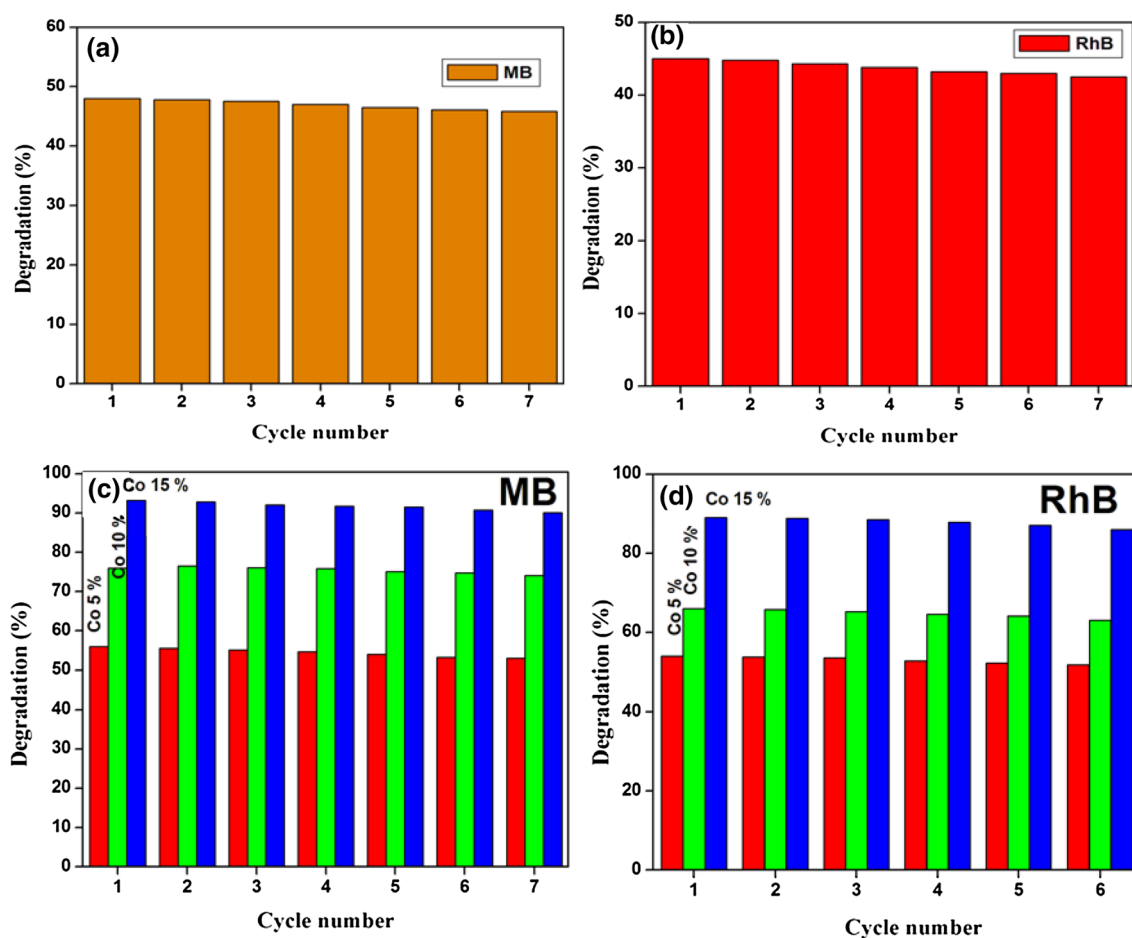


Fig. 7 Recycling cycles of test of **a** MB and **b** RhB using pure CdS catalyst; **c** MB and **d** RhB using Co doped CdS catalyst under visible light irradiation

photo-stability of the photocatalyst for seven cycles without a major reduction in photo-activity. After seven cycles, the Co-CdS showed a negligible reduction in photocatalytic activity and more than 90% degradation was attained. The reusability test of the Co-CdS photocatalyst showed high photo stability with a low photo-corrosive effect. The catalyst showed a slight decrease in efficiency due to incomplete recollection and loss during the washing process. Hence, this type of catalyst powders might be a promising potential application in waste water treatment.

Photocatalytic mechanism

The detailed photocatalytic mechanism of the Co-CdS catalyst powder under visible light is discussed in Fig. 8. Generally, the photocatalytic activity of the photocatalysts can be influenced by various factors, such as porosity, composition, band gap, crystallite nature, surface hydroxyl density, specific surface area, photo-generated charge separation efficiency and particle size distribution [26]. In our case, the

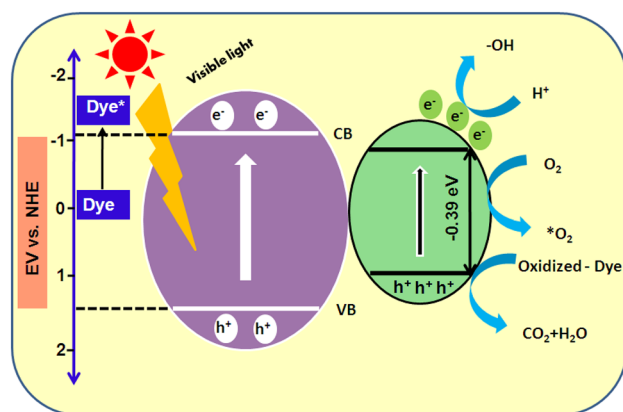


Fig. 8 Schematic representation for photocatalytic mechanism of Co-doped CdS catalyst under visible light irradiation

insertion of Co²⁺ has improved the photocatalytic activity of CdS nanostructures significantly. It can be moderately ascribed to the differences in crystallite size and structural

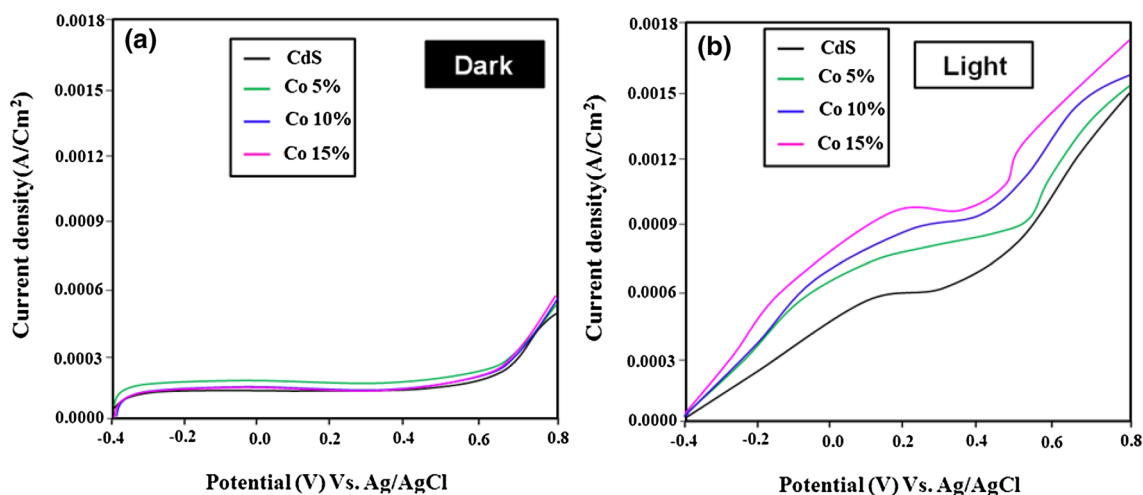


Fig. 9 Current density versus applied potential curves of photoelectrochemical measurement; **a** dark, **b** light

morphology of the synthesized samples with doping concentration. The highest photocatalytic activity is found for 15% Co-doped CdS nanostructures, which may be accredited to the accessibility of large number of spherical nanoparticles having higher value of surface to volume ratio in comparison to other samples. Since band gap energy is lowered in Co-doped CdS samples compared with pristine CdS, the energy of visible light can generate more e^-h^- couples resulting in the higher photocatalytic activity.



In the schematic illustration, photo-generated electrons are transferred from the valence band to the conduction band of undoped CdS under visible light illumination. The electrons localized from the conduction band (CB) of CdS transfer to the CB of Co–CdS, while the holes stored in the VB of CdS are trapped by sacrificial agents. As a result, the photo-generated charge recombination can be decreased, leading to an enhanced photoactivity compared with pure CdS [27, 28]. In Co-doped CdS, substitution of Co^{2+} ions with Cd^{2+} ions in CdS host lattice lowers the conduction band of CdS. As a result, in Co-doped CdS samples, electrons can be excited simultaneously from the valence band to Co energy level. In addition, the photo-generated electrons can easily be transferred from the conduction band and the Co doping energy level to the surface of photocatalyst to capture adsorbed O_2 which improves separation efficiency of charge carriers. During the photocatalytic reaction, the reduction of CO_2 is varied from the proton-assisted multiple-electron transfer process. The gas products may include CO , CH_4 , and C_2H_6 , and the liquid hydrocarbons may contain HCOOH , HCHO and CH_3OH . The product selectivity is strongly influenced by the photoactive materials in the Co-CdS photocatalysts [29]. These two mechanisms give rise to

the increase in photocatalytic efficiency by 15% Co-doped CdS catalyst as compared to undoped CdS samples.

Photoelectrochemical studies

In this study, PEC measurements were studied in a three-electrode cell connected to a CHI 660D work station (CH Instrument) at $\sim 30^\circ\text{C}$. An earlier study showed that Co-doped CdS with good photocatalytic activity should possess the following material-related characteristics: good crystallinity and large surface area and smaller band gap energy. Figure 9 shows the photoelectrochemical characteristic curve of pure and Co-doped CdS nanoparticles. The Ag/AgCl ($0.2 \text{ mol L}^{-1} \text{ Na}_2\text{SO}_4$ -filled) and a platinum wire (Pt) were used as the working, reference, and counter electrodes for the ohmic contact. When the applied voltage was gradually increased from -0.6 to 1.2 V , the CdS curve (dark) was almost a straight line. Under Xe-lamp illumination, the photocurrent density of both pure and Co-doped CdS samples showed improvement over that without illumination. These results showed that the photo-current density of the Co-doped CdS nanoparticles increased by at least three times at the same applied voltage ($E = 1.25 - 0.055 \times \text{PH} (\text{Na}_2\text{SO}_4, 6.8) - 0.1745 \text{ Ag/AgCl}$) than pure CdS.

Conclusion

Using wet chemical synthesis technique, we have successfully synthesized nano-dimensional CdS:Co particles without any capping agent. All the experimental analyses confirmed the incorporation of Co into CdS. The XRD and TEM results suggest that Co-doped CdS was single cubic structure and average particle sizes were around 16–28 nm.

The optical absorption studies revealed that incorporation Co altered the optical band gap of the CdS nanoparticles. A relatively high photodegradation activity was observed for 15% Co-doped CdS nanostructures due to their high interacting surface area for dye molecules. The improved photocatalytic activity of Co-doped samples may be due to the presence of doping-induced impurity levels within the band gap which may help in prolonging the recombination time of electrons and holes, resulting in enhanced photocatalytic degradation of MB dye.

Compliance with ethical standards

Conflict of interest The authors declare that there is no conflict of interest regarding the research work reported in this manuscript.

References

1. H.M. Gibbs, G. Khitrova, in *Semiconductor Nanocrystals for Non-Linear Optical Devices*, In *Non-Linear Photoionics*, ed. by H. Gibbs, G. Khitrova, N. Peyghambarian (Springer, Berlin, 1990)
2. S.V. Gaponenko, *Optical Properties of Semiconductor Nanocrystals* (Cambridge Univ. Press, Cambridge, 1998)
3. I. Ekimov, A.L. Efros, *Phys. Status Solidi B* **150**, 627 (1988)
4. L.E. Brus, *Appl. Phys. A* **53**, 465 (1991)
5. D.H. Kim, D.J. Lee, N.M. Kim, S.J. Lee, T.W. Kang, Y.D. Woo, D.J. Fu, *J. Appl. Phys.* **101**, 094111 (2007)
6. K.W. Liu, J.Y. Zhang, D.Z. Shen, X.J. Wu, B.H. Li, B.S. Li, Y.M. Lu, X.W. Fan, *Appl. Phys. Lett.* **90**, 092507 (2007)
7. C.W. Na, D.S. Han, D.S. Kim, Y.J. Kang, J.Y. Lee, J. Park, D.K. Oh, K.S. Kim, D. Kim, *J. Phys. Chem. B* **110**, 6699 (2006)
8. M. Tambidurai, N. Muthukumarasamy, S. Agilan, N. Murugan, N. Sabari Arul, S. Vasantha, R. Balasundaraprabhu, *Solid State Sci.* **12**, 1554 (2010)
9. A.R. Chauhan, R. Kumar, P. Chaudhary, *Res. Chem. Intermed.* **39**, 645 (2013)
10. I.F. Ertis, *Int. J. Chem. React. Eng.* **15**, 1 (2016)
11. A.M. Abdulkarem, E.M. Elssfah, N.N. Yan, G. Demissie, Y. Yu, *J. Phys. Chem. Solids* **74**, 647 (2013)
12. M. Tambidurai, N. Muthukumaraswamy, D. Velayuthapillai, S. Agilan, R. Balasundaraprabhu, *Powder Technol.* **217**, 1 (2012)
13. M. Tambidurai, N. Muthukumaraswamy, D. Velayuthapillai, S. Agilan, R. Balasundaraprabhu, *J. Electron. Mater.* **41**, 665 (2012)
14. L. Saravanan, A. Pandurangan, R. Jayavel, *J. Nanopart. Res.* **13**, 1621–1628 (2011)
15. M. Tingtinghu, S. Zhang, G. Wang, S. Cui, Sun, *Cryst. Engg. Comm.* **13**, 5646 (2011)
16. M.B. Leena, K. Raji, *Int. J. Adv. Eng. Res. Dev.* **4**, 1 (2017)
17. M. Parthibavarman, K. Vallalperuman, S. Sathishkumar, M. Durairaj, K. Thavamani, *J. Mater. Sci. Mater. Electron.* **25**, 730 (2014)
18. D. Madhan, M. Parthibavarman, P. Rajkumar, M. Sangeetha, *J. Mater. Sci. Mater. Electron.* **26**, 6823 (2015)
19. R. Gao, L. Wang, Y. Geng, B. Ma, Y. Zhu, H. Dong, Y. Qiu, *J. Phys. Chem. C* **115**, 17986 (2011)
20. P. Koidl, *Phys. Rev. B* **15**, 2493 (1977)
21. M. Parthibavarman, B. Renganathan, D. Sastikumar, *Curr. Appl. Phys.* **13**, 1537 (2013)
22. S. Kumar, Z. Jindal, N. Kumari, N.K. Verma, *J. Nanopart. Res.* **13**, 5465 (2011)
23. N.V. Hullavarad, S.S. Hullavarad, *J. Vac. Sci. Technol. A* **26**, 1050 (2008)
24. M. Lazell, P. O'Brien, *J. Mater. Chem.* **9**, 1381 (1999)
25. M. Parthibavarman, S. Sathishkumar, S. Prabhakaran, *J. Mater. Sci. Mater. Electron.* **29**, 2341 (2018)
26. K. Hu, X. Hu, Y. Xu, J. Sun, *J. Mater. Sci.* **45**, 2640 (2010)
27. L. Yuan, M.-Q. Yang, Y.-J. Xu, *Nanoscale* **6**, 6335 (2014)
28. N. Zhang, M.-Q. Yang, S. Liu, Y. Sun, Y.-J. Xu, *Chem. Rev.* **115**, 10307 (2015)
29. Y.-S. Xie, L. Yuan, N. Zhang, Y.-J. Xu, *Appl. Catal. B* **238**, 19 (2018)